CFD Simulations of Non-Linear Sloshing in a Rotating Rectangular Tank Using The Level Set Method

Erlend Liavåg Grotle*[1], Hans Bihs[2], Vilmar Æsøy[1], and Eilif Pedersen[3]

[1]Faculty of Marine Technology and Operations, Norwegian University of Science and Technology (NTNU), °Alesund, Norway
[2]Department of Civil and Environmental Engineering, Norwegian University of Science and Technology (NTNU), 7491 Trondheim, Norway
[3]Department of Marine Technology, Norwegian University of Science and Technology (NTNU), 7491 Trondheim, Norway

Journal of Offshore Mechanics and Offshore Engineering, 2018, **140** ()6), pp. 61806.
DOI: http://dx.doi.org/10.1115/1.4040560

Abstract

In this paper, numerical simulations of non-linear sloshing in rectangular tanks are presented. Model implementations in the open source software REEF3D are tested and results compared with experimental data with three different conditions. The interface location is compared for both linear and non-linear sloshing. The non-linear sloshing is simulated in both 2D and 3D. Video images from the SPHERIC project are compared with simulations for the interface. A condition with lateral wave impacts in sloshing, with a frequency close to the natural frequency of the first mode, can be found in this case. The numerical model is solving the RANS equations with the $k-\omega$ turbulence model. The level set method is used to capture the interface. Higher order discretization schemes are implemented to handle time-evolution and convective fluxes. A ghost cell method is used to account for solid boundaries and parallel computations. It is found that the limiting factor for the eddy-viscosity has significant influence in the non-linear sloshing cases. As the sloshing becomes more violent, the increased strain at the gas-liquid interface overproduces turbulence energy with unrealistically high damping of the motion. 3D simulations show slightly better comparison than 2D. Due to non-linearities and small damping, the time to reach steady-state may take several cycles. The last case shows promising results for the global motion. As expected, the break up of the liquid surface makes it difficult to resolve each phase. But overall, the numerical model predicts the sloshing motion reasonably well.

*Corresponding author,grotle@ntnu.no
Postprint, published in Journal of Offshore Mechanics and Offshore Engineering, doi:http://dx.doi.org/10.1115/1.4040560

1 Introduction

Traditionally, forces and moments have been the main concern in studies of sloshing tanks. This is due to strength requirements on transport tanks and stability on ships with roll-stabilizing tanks. Other problems concerned with sloshing are increased rate of boil-off gas in transport tanks with oil or cryogenic liquids. In recent years, there have been studies related to the pressure drop inside pressurized cryogenic fuel tanks. The same issue is now faced within the maritime sector with an increasing number of LNG fuelled ships. The main reason for this is believed to be enhanced mixing of liquid and gas at the interface. In Satoru et al. (1982) the turbulence structure at the interface is investigated and shows that turbulent eddies close to the integral length scale are the driving mechanism for heat and mass transfer at the interface.

This paper presents studies of numerical simulations of non-linear sloshing. This is important because accurate representation of thermal mixing in the tanks relies on an accurate representation of the flow field. Extensive information about sloshing and how to approach it analytically can be found in Faltinsen and Timokha (2009). The simulation cases used for validation in this paper can be found in La Rocca et al. (2000), which models sloshing with the variational method. The model predicts accurate results compared to the experiments. With analytical based methods, the flow field cannot be modelled in detail when the sloshing becomes violent. CFD is a suitable tool for this purpose, but should not be used without concern regarding the treatment of turbulence modelling.

The numerical model REEF3D is based on solving the velocity field using the Reynolds-averaged Navier-Stokes equations (RANS). The model has been extensively used for wave hydrodynamics problems Chella et al. (2015), ocean wave energy Kamath et al. (2015) and sediment transport problems Afzal et al. (2015). The k-ω model Wilcox (1994) is used to close the set of equations. The model is based on a one-fluid approach and the entire domain is solved as if it was one phase. This creates large strains at the interface, and the turbulence energy easily gets overproduced. This results in unrealistically large values of the eddy-viscosity, which dampens the mean velocity field in this region. Few studies of turbulence modelling involving a gas-liquid interface using conventional two-equation turbulence models can be found. Turbulence modelling of hydraulic engineering applications are studied in Rodi (1993) and Naot and Rodi (1982). Generally, the effect of the gas-liquid interface on turbulence is similar to that of a solid wall, prohibiting the turbulent length scale from transitioning across the interface. A general limiter on eddy-viscosity is used in this work Durbin (2009), and also a boundary condition of ω at the interface.

2 Mathematical Models and Numerical Methods

The flow is assumed incompressible with constant density and molecular viscosity in the gas and liquid phase. Hence, compressibility and thermal effects are neglected. The governing equations are solved numerically using a finite difference method. One set of equations describes the entire flow field, with immersed boundaries inside the domain. The method used here is not restricted to rectangular tanks, but many studies are based on this geometry, and it excludes extensive complications of fluid-solid boundaries.

2.1 Basic Equations

We assume incompressible flow and a Newtonian fluid. Splitting into averaging and fluctuating terms, gives the simplified RANS equation Wilcox (1994):

$$\frac{\partial \overline{u}_i}{\partial t} + \overline{u}_j \frac{\partial \overline{u}_i}{\partial x_j} = -\frac{1}{\rho}\frac{\partial \overline{p}}{\partial x_i} + \frac{\partial}{\partial x_j}\left[(\nu + \nu_t)\left(\frac{\partial \overline{u}_i}{\partial x_j} + \frac{\partial \overline{u}_j}{\partial x_i}\right)\right] + \overline{f}_i \tag{1}$$

Where ν_t is the turbulence eddy-viscosity. The last term is body forces. Since we are using a tank-fixed coordinate system, source terms in addition to gravity must be accounted for to represent the equations in a non-inertial global system. These are given as:

$$\begin{aligned} \overline{f}_x &= \ddot{\theta}(y - y_m) + \dot{\theta}^2(x - x_m) - g sin\theta, \\ \overline{f}_y &= -\ddot{\theta}(x - x_m) + \dot{\theta}^2(y - y_m) - 2\dot{\theta}\ \overline{u} - g cos\theta. \end{aligned} \tag{2}$$

where the y-component is the vertical direction (see Fig. 1) and x is in the longitudinal direction of the tank (along L). As the motion is planar, no source term is added for the y-component. θ is the rotational angle. $\dot{\theta}$, $\ddot{\theta}$ is angular velocity and acceleration respectively. The coordinates x_m and y_m lies in the center of the rotational point, and therefore $x - x_m$ is the distance from the rotational point to the center of the tank fixed coordinate system. The second last term of the y-component is the *Coriolis* acceleration.

2.2 Turbulence Modelling

Modelling turbulence in sloshing, or general moving interface flows with large density ratios, is a complex task. To calculate the velocities and pressure of Eq. (1), an expression for the eddy-viscosity is needed. The two-equation, k-ω turbulence model, is used to close the set of equations Wilcox (1994). These are the kinetic turbulence energy and the specific dissipation rate of turbulence energy, ω. The equations can be written Wilcox (1988):

$$\frac{\partial k}{\partial t} + \overline{u}_j \frac{\partial k}{\partial x_j} = \frac{\partial}{\partial x_j}\left[\left(\nu + \frac{\nu_t}{\sigma_k}\right)\frac{\partial k}{\partial x_j}\right] + P_k - \beta_k k\omega \tag{3}$$

$$\frac{\partial \omega}{\partial t} + \overline{u}_j \frac{\partial \omega}{\partial x_j} = \frac{\partial}{\partial x_j}\left[\left(\nu + \frac{\nu_t}{\sigma_\omega}\right)\frac{\partial \omega}{\partial x_j}\right] + \frac{\omega}{k}\alpha P_k - \beta\omega^2 \tag{4}$$

P_k is the turbulence energy production term. σ_k, σ_ω are standard coefficients in the model, both with values equal to 2 in this case. β_k, β and α are empirical constants, with values 9/100, 3/40 and 5/9 respectively. The RANS model overproduces the turbulence energy in highly strained flows. This gives unrealistically large values for the eddy-viscosity. Menter Menter (1994) noted that the stress intensity ratio scales with the ratio of turbulence production to dissipation. Typical stress intensity ratios can be found from experiments in certain type of flows. In order to avoid overproduction of turbulence in highly strained flow outside the boundary layer, the turbulence eddy-viscosity, ν_t, can be bounded through the limiting formulation Durbin (2009):

$$\nu_t = \min\left(\frac{k}{\omega}, \sqrt{\frac{2}{3}}\frac{k}{|\mathbf{S}|}\right) \tag{5}$$

where **S** is the square root of rate of strain magnitude.

The rough wall function by Schlichting Schlichting (1979) is applied to all the wall boundaries Bihs et al. (2016):

$$u^+ = \frac{1}{\kappa} ln \left(\frac{30y}{k_s} \right). \tag{6}$$

u^+ is the dimensionless wall velocity, κ is a constant equal to 0.4, y the water depth and k_s is the equivalent sand roughness. Near the wall it is assumed that the turbulent production is equal to the dissipation of turbulent energy. The wall function for the specific turbulent dissipation ω for a bed cell with the distance Δy_p from the wall to the center of the cell is then:

$$\omega_{wall} = -\frac{C_\mu^{3/4} k_w^{1/2} u_w^+}{\Delta y_p}, \tag{7}$$

The formula gives the value for ϵ directly. The turbulent kinetic energy k at the wall is treated by integrating the source terms of Eq. 3 over the bed cell:

$$\int \left(P_k - \epsilon_w \right) \rho = \left[\frac{\tau_w u_w}{\Delta y_p} - \frac{\rho C_\mu^{3/4} k_w^{3/2} u_w^+}{\Delta y_p} \right]. \tag{8}$$

The rough wall law is then used to determine the wall shear stress τ_w and the dimensionless u^+. The terms from Eq. 8 are discretized as source terms in the transport equation for k.

At the gas-liquid interface it seems plausible that the turbulence length scales are reduced, at least for the velocity component normal to the gas-liquid interface. This is due to similar effects as on wall boundaries, where a shear layer is formed due to forces near the surface. The normal fluctuations are damped out, with an amplification of the other components. It is assumed by the $k-\omega$-turbulence model that the turbulence is isotropic, while in reality it is likely to be anisotropic at the interface. A boundary condition is proposed to limit the length scale near the interface Naot and Rodi (1982):

$$\omega_s = \frac{C_\mu^{-1/4}}{\kappa} k^{1/2} \cdot \frac{1}{y'} \tag{9}$$

where $C_\mu = 0.07$ and $\kappa = 0.4$. y' is the virtual origin of the length scale of the turbulence. In Hossain and Rodi (1980) this was determined to be 0.07 times the mean water depth. To activate this boundary condition at the interface of thickness ϵ, the expression is multiplied by the Dirac delta function:

$$\delta(\phi) = \begin{cases} \frac{1}{2\epsilon} \left[1 + \cos\left(\frac{\pi\phi}{\epsilon} \right) \right], & \text{if } |\phi| < \epsilon; \\ 0, & \text{otherwise} \end{cases} \tag{10}$$

where ϕ is the level set function. The requirement for a Dirac delta function to be valid is that ϵ approach zero.

It should be noted that Eq. 5 is a general limiter of the eddy-viscosity. The interface boundary condition for ω in Eq. 9 increases the dissipation and therefore reduces the eddy-viscosity, but only at the interface. Any reduction of y' increases ω, and therefore increases the damping of the eddy-viscosity. In the cases simulated here, the results indicate that the factor y' is somewhat too low. But more systematic studies are required to make a conclusion.

2.3 Interface Capturing

The interface between liquid and gas represent a discontinuity in the field. To capture the interface, the level set technique is used, first presented by Osher and Sethian (1988). The location of the surface is represented by the zero level of a signed distance function. The following properties are defined:

$$\phi(\mathbf{x},t) = \begin{cases} > 0, & \text{if } \mathbf{x} \in \text{phase 1;} \\ = 0, & \text{if } \mathbf{x} \in \Gamma; \\ < 0, & \text{if } \mathbf{x} \in \text{phase 2} \end{cases} \tag{11}$$

Where Γ is at the gas-liquid interface. In order to move the interface inside a velocity field, the level set function, ϕ, is convected using the equation

$$\frac{\partial \phi}{\partial t} + \overline{u}_j \frac{\partial \phi}{\partial x_j} = 0 \tag{12}$$

When the level set function is moved, it will not remain a signed distance function. For this to be fulfilled it must satisfy the Eikonal equation to ensure mass conservation. Reinitialization at each time step is done using a PDE based equation Sussman et al. (1994), Peng et al. (1999). Treatment of the abrupt change of fluid properties is needed, and to avoid numerical instabilities, the values are smoothed across the interface. This can be done by assigning a finite thickness to the interface. The thickness is 2ϵ, and is given a value equal to $\epsilon = 2.1\Delta x$, where Δx is the grid spacing. Smoothening in this region is carried out with a Heavyside function, $H(\phi)$. Once the function is obtained, the fluid densities and viscosities can be calculated:

$$\begin{aligned} \rho(\phi) &= \rho_1 H(\phi) + \rho_2 \left[1 - H(\phi)\right] \\ \mu(\phi) &= \mu_1 H(\phi) + \mu_2 \left[1 - H(\phi)\right] \end{aligned} \tag{13}$$

2.4 Discretization and Solving

Chorin's projection method Chorin (1968) is used to handle the pressure-velocity coupling. This procedure starts with computing an intermediate velocity field by ignoring the pressure terms in the RANS equations. This is the predictor step. In the next projection step the pressure gradient is added to give the final velocity at the next time step. The continuity condition is used to eliminate $\overline{u}^{n+1}$, to get the Poisson equation:

$$\frac{\partial}{\partial x_i}\left(\frac{1}{\rho}\frac{\partial p}{\partial x_i}\right) = -\frac{1}{\Delta t}\frac{\partial \overline{u}_i^*}{\partial x_i}, \tag{14}$$

where $\overline{u}_i^*$ is the intermediate velocity found in the predictor step. When the new pressure field is found, the divergence-free velocity can be calculated. This equation is solved using the fully parallelized Jacobi-preconditioned BiCGStab algorithm Van der Vorst (1992).

Convective terms in the RANS equation are discretized using the conservative fifth-order WENO scheme Jiang and Shu (1996). A non-conservative WENO scheme (Weno HJ) is used to discretize the convective terms in the level set equation and the k and ω equations. General information about the ENO schemes to discretize the level set function is found in Osher and Fedkiw (2006). Essentially non-oscillatory (ENO) schemes bring higher order to the first order upwind schemes by polynomial interpolation of the flux functions. There are three possible HJ ENO approximations to the fluxes. The weighted essentially non-oscillatory scheme (WENO) uses a weight parameter to combine the three stencils. All temporal discretization is done with third order TVD Runge-Kutta scheme Harten (1983), except for the turbulence model equations. Adaptive time stepping ensures that the CFL criteria is fulfilled.

The grid is uniform and orthogonal. Construction of this is done quite easily in a rectangular domain. The ghost cell method Berthelsen and Faltinsen (2008) is implemented to account for solid boundaries, and is also used to handle multi-directional ghost cells.

3 Simulation Cases and Results

Three different test cases have been simulated and compared with experiments. The first two test cases (case 1 and 2) are collected from experiments performed by La Rocca et. al, and presented in La Rocca et al. (2000). A three-dimensional rectangular container is simulated representing both linear and non-linear sloshing regimes. This is done by keeping the amplitude and liquid depth constant, only varying the frequency. The experiments are suitable for both 2D and 3D simulations, in which 3D is performed only in case 2. The SPHERIC project Botia Vera et al. (2010) is used as a third test case. This has different geometrical parameters than the first two cases. The geometrical definitions are summarized in Fig. 1 with data in Tab. 1. The periodic rotational motion of the tank is prescribed and the angle is equal to

$$\theta(t) \approx Amp \cdot sin(\omega t), \tag{15}$$

where Amp is the rotational amplitude, ω the frequency and t is time. The test parameters are summarized in Tab. 2, where h is the depth, L length of the tank and ω_{01} the natural frequency of the first mode. The total number of motion periods run in the simulations is also given, which is the forcing frequency times the simulation time. The fluid properties are equal to those of air and fresh water at standard atmospheric conditions. All cases have a rotational axis parallel to the axis in the transversal direction at the middle bottom of the tank as illustrated in Fig. 1. The numerical set-up is similar to the experimental, as shown in Fig. 1, always with the same length L and height H. 2D-simulations are performed by cutting the box in the x-y plane with a resulting domain with 1 cell thickness in the z-direction. Symmetry is employed on both surfaces in the x-y plane. All other surfaces are no-slip walls. In the 3D simulations, the numerical domain is exactly the same as shown in Fig. 1 with a uniform grid and no-slip walls. The cell size is uniform and equal in all directions.

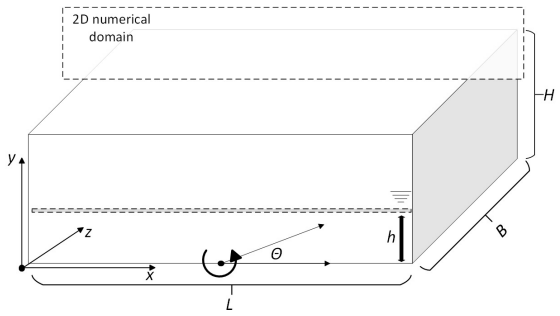

Figure 1: Tank layout.

Table 1: Tank dimensions.

Case	L[m]	B[m]	H[m]
1	0.50	0.50	0.25
2	0.50	0.50	0.25
3	0.90	0.05	0.58

3.1 Grid-sensitivity study

A sensitivity study is performed by simulating case 2 in 2D. The result is shown in Fig. 2 and is not very different considering that the great difference in cell numbers. The different computational time between $\Delta x = 0.002$ and $\Delta x = 0.003$ were extensive so it was decided to proceed with the middle alternative with 13889 cells. The domain in case 3 is larger, and to limit the computational time it was decided to use $\Delta x = 0.004$. This case requires more cells to resolve the splashing, but no aim was done to fully resolve this.

3.2 2D Validation Cases

The liquid depth of the cases 1 and 2 corresponds to the region of intermediate depths for water waves. Case 2 has a non-linear regime. It shows unstable 2D configurations of the interface and particularly sensitive to disturbances at the beginning of the motion. The experimental results are assumed to be steady-state, although each of the few cycles show some differences. The 2D numerical domain is illustrated with a plane cut along the x-direction in Fig. 1.

Fig. 3 shows the wave elevation at point $x = 0.15$ and $z = B/2$. As expected, in the linear sloshing regime (case 1), the wave-elevation shows acceptable agreement with experimental data as shown in Fig. 3. Turbulence modelling is included, but without the interface boundary condition for ω in Eq. 9.

Simulation results from case 2 are shown in Fig. 4. Without the gas-liquid interface boundary condition for ω, the higher order oscillations are damped out, with amplification of the first mode. By introducing the boundary condition of turbulence dissipation in Eq. (9), less damping of the wave elevation is found. The non-linearity of the motion is clearly depending

Table 2: Validation test parameters.

Case	Amp[°]	h/L	ω/ω_{01}	No. of cycles
1	4.985	0.272	0.29	10
2	4.985	0.272	0.67	30
3	3.875	0.103	0.85	18

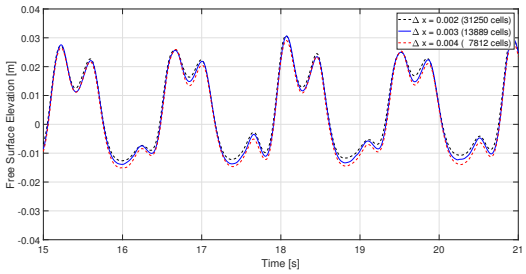

Figure 2: Comparison of grid spacing.

on the turbulence modelling settings, which is probably one of the most crucial element in modelling the gas-liquid interface correctly. As stated in La Rocca et al. (2000), the third mode natural frequency is close to 3 times the forcing frequency which results in third order resonance. Since there is no wave breaking taking place in this case, the damping is governed by shear forces at the gas-liquid interface and walls. No information about the actual platform motion is given in La Rocca et al. (2000), and to avoid initial disturbances, there might be a ramp-up of the forcing frequency. Due to the intermediate level with higher order oscillations, and the absence of wave breaking, the steady-state condition may take several cycles. An initial deviation of the forcing frequency may change the sloshing characteristics for some cycles, due to the unstable characteristics. The number of cycles to reach steady-state may be a indicator of how accurate the turbulence is modelled.

3.3 3D Simulations of Case 2

The same settings are applied to the 3D simulations of case 2. Experimental data are found from the same paper La Rocca et al. (2000). A simulation of 25 cycles were performed, which corresponds to approximately 35 seconds. The wave-elevation from the 3D simulations can be found in Fig. 5. The 2D results are also given. It can be seen that after 25 seconds, the simulation results are quite similar, but the experimental results are clearly different from both the 2D and 3D. The numerical results in La Rocca et al. (2000) are also very similar. As stated by La Rocca et. al, the main difference between 2D and 3D in case 2, is the greater spectral contribution of a frequency that is three times the forcing frequency. The fact that the simulation results are so close, may indicate that the 3D effects are dampened out. If this is related to turbulence modelling settings or not is difficult to state.

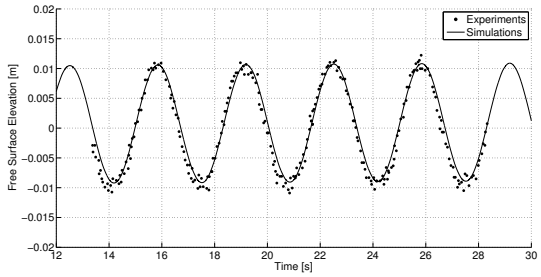

Figure 3: Wave elevation in case 1.

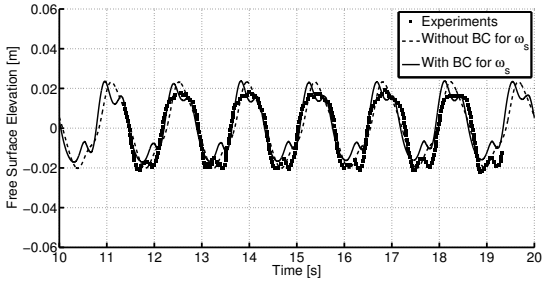

Figure 4: 2D simulations of case 2.

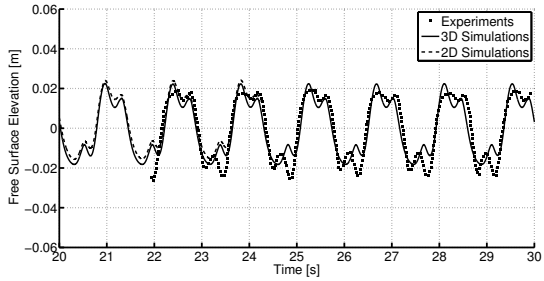

Figure 5: 3D simulations of case 2.

3.4 Simulations of Case 3

In the third case the water depth is shallow, creating overturning and breaking waves, and also lateral wave impacts on the side walls. In Fig. 6, video files from experiments are patched onto simulation results in case 3. The series of images in Fig. 6 shows the progress of a spilling breaker before it hits the wall. Fig. 8 shows when a wave hits the wall. The overall motion of the liquid is captured acceptably. Once the liquid hits the wall and breaks into pieces, there is a slight discrepancy. The case is transient, and no long simulation runs are required to compare. Steady state is reached relatively fast, as the damping is higher.

Fig. 7 and Fig. 9 show contour and vector plots of the velocity field from case 3. It is

interesting to observe how the air is influenced by the liquid sloshing. In Fig. 7, the spilling breaker is shown. It can be observed how the front pushes the air which is sucked back into the backside of the water wave. Fig. 9 shows the impact. After some cycles, the liquid sloshing induces vortexes in the air phase. To the left in Fig. 9, the vortex is a result from the previous cycle, while a new vortex is generated at the top right of Fig. 9 c.

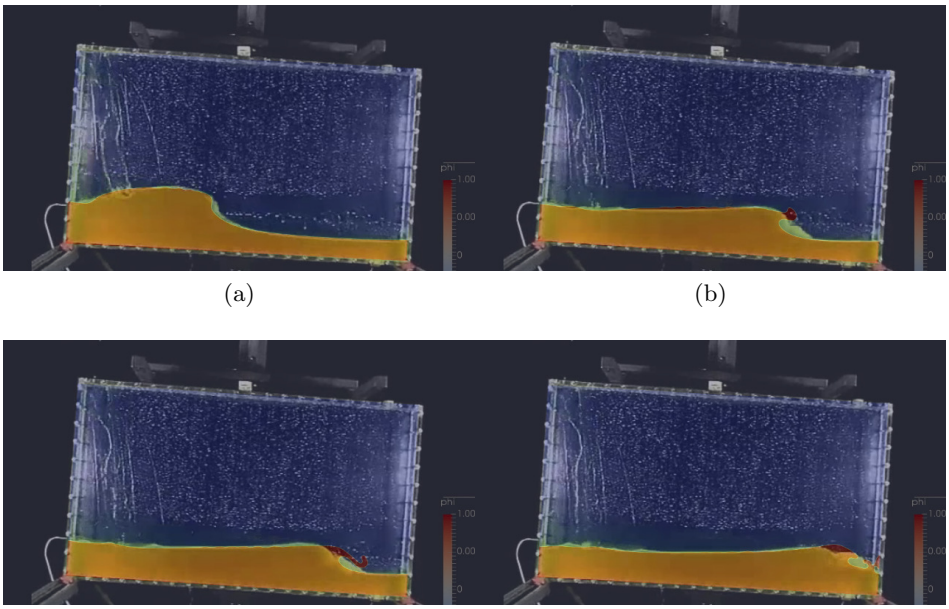

(a) (b)

(c) (d)

Figure 6: Case 3 - video captions of experiments and simulations showing a spilling breaker. (permission from the authors of Botia Vera et al. (2010)).

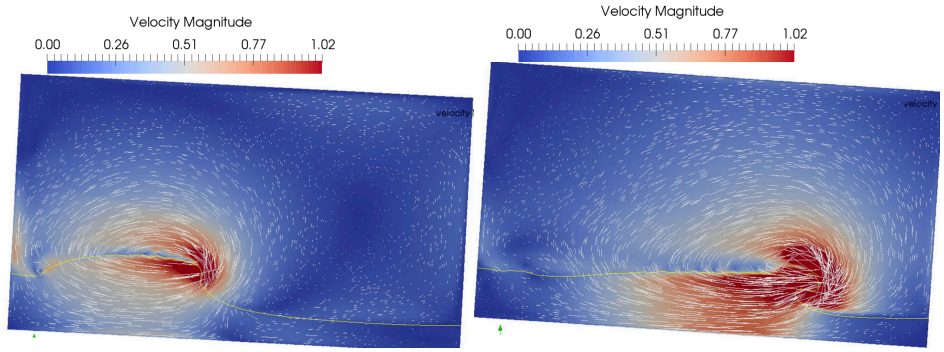

(a) (b)

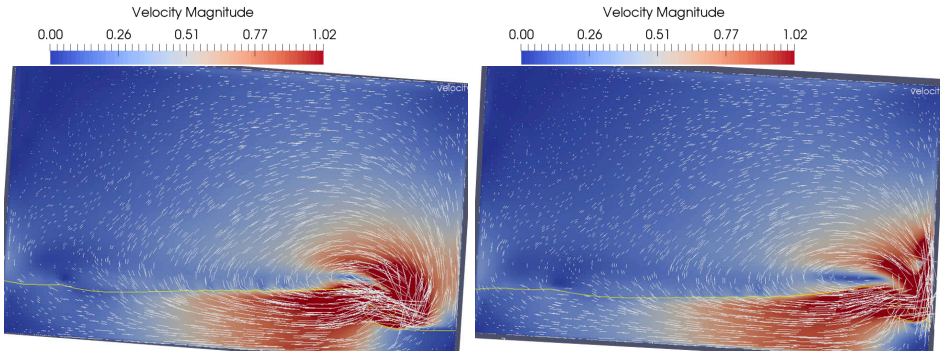

(c) (d)

Figure 7: Case 3 - velocity field of a spilling wave.

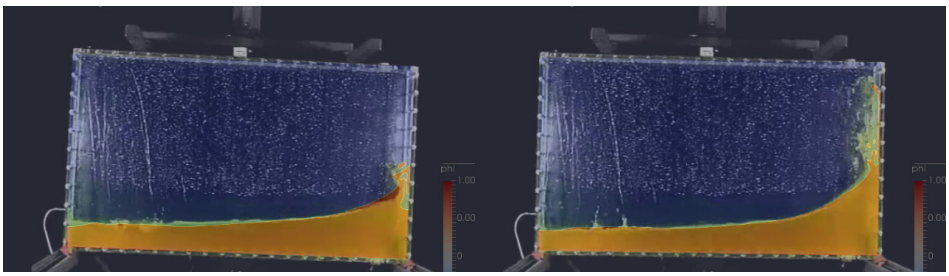

(a) (b)

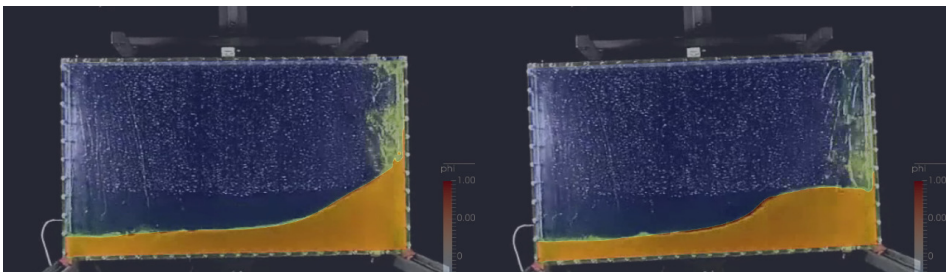

(c) (d)

Figure 8: Case 3 - video captions of wave impact.

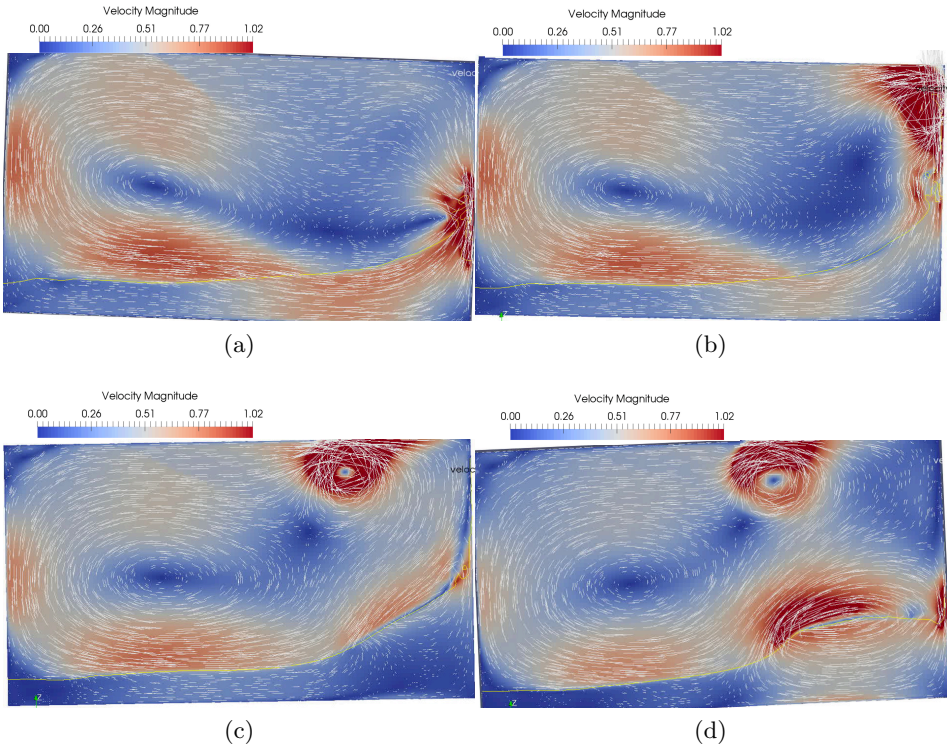

Figure 9: Case 3 - velocity field of wave impact.

4 Conclusion

Three different sloshing cases are simulated and compared with experiments. The first case shows that the numerical model matches the experimental results. All the test cases are quite different. Case 2 has a marked non-linear behaviour, but without breaking of the waves. Case 3 has spilling breakers and lateral impacts. The results indicate that the non-linear behaviour in sloshing is dependening on the turbulence model settings. This makes it interesting to investigate sloshing characteristics other than violent sloshing, and even cases that can be simulated satisfactorily with analytical approaches, like in La Rocca et al. (2000). If higher order oscillations occur, and these do not contain wave breaking, the dissipation is smaller, and the steady-state condition may take several cycles. The relation between turbulence modelling and the steady-state behaviour in experiments should be investigated more thoroughly. The results from this work indicate that the virtual origin of the turbulent length scale in Eq. 9 should be somewhat greater. Other sloshing cases should be investigated systematically. The results from case 3 show that the level set method predicts the violent sloshing quite well. This case also demonstrates the ability of REEF3D to investigate challenging sloshing cases, and provides insight of the whole domain in a sloshing tank, like details of the gas phase velocity field. All in all the results are promising, and justify the use of conventional turbulence models and the level set method to simulate sloshing flows.

References

Afzal, M.S., Bihs, H., Kamath, A. and Arntsen, Ø.A. (2015). Three-dimensional numerical modeling of pier scour under current and waves using level-set method. *Journal of Offshore Mechanics and Arctic Engineering*, **137**(3), 032001.

Berthelsen, P.A. and Faltinsen, O.M. (2008). A local directional ghost cell approach for incompressible viscous flow problems with irregular boundaries. *Journal of computational physics*, **227**(9), 4354–4397.

Bihs, H., Kamath, A., Alagan Chella, M., Aggarwal, A. and Arntsen, Ø.A. (2016). A new level set numerical wave tank with improved density interpolation for complex wave hydrodynamics. *Computers & Fluids*, **140**, 191–208.

Botia Vera, E., Souto Iglesias, A., Bulian, G. and Lobovskỳ, L. (2010). *Three SPH Novel Benchmark Test Cases for free surface flows.* University of Manchester, Manchester, UK.

Chella, M.A., Bihs, H., Myrhaug, D. and Muskulus, M. (2015). Breaking characteristics and geometric properties of spilling breakers over slopes. *Coastal Engineering*, **95**, 4–19.

Chorin, A.J. (1968). Numerical solution of the Navier-Stokes equations. *Mathematics of Computation*, **22**(104), 745–762.

Durbin, P.A. (2009). Limiters and wall treatments in applied turbulence modeling. *Fluid Dynamics Research*, **41**(1), 012203.

Faltinsen, O.M. and Timokha, A.N. (2009). *Sloshing.* Cambridge University Press, Cambridge, UK.

Harten, A. (1983). High resolution schemes for hyperbolic conservation laws. *Journal of Computational Physics*, **49**(3), 357–393.

Hossain, M. and Rodi, W. (1980). Mathematical modelling of vertical mixing in stratified channel flow. In: *Proceedings of the 2nd Symposium on Stratified Flows, Trondheim, Norway*, 280–290.

Jiang, G. and Shu, C. (1996). Efficient implementation of weighted ENO schemes. *Journal of Computational Physics*, **126**(130), 202–228.

Kamath, A., Bihs, H. and Arntsen, Ø.A. (2015). Numerical modeling of power take-off damping in an oscillating water column device. *International Journal of Marine Energy*, **10**, 1–16.

La Rocca, M., Sciortino, G. and Boniforti, M.A. (2000). A fully nonlinear model for sloshing in a rotating container. *Fluid Dynamics Research*, **27**(1), 23.

Menter, F.R. (1994). Two-equation eddy-viscosity turbulence models for engineering applications. *AIAA journal*, **32**(8), 1598–1605.

Naot, D. and Rodi, W. (1982). Calculation of secondary currents in channel flow. *Journal of the Hydraulics Division*, **108**(8), 948–968.

Osher, S. and Fedkiw, R. (2006). *Level set methods and dynamic implicit surfaces*, volume 153. Springer, New York, USA.

Osher, S. and Sethian, J.A. (1988). Fronts propagating with curvature-dependent speed: algorithms based on hamilton-jacobi formulations. *Journal of Computational Physics*, **79**(1), 12–49.

Peng, D., Merriman, B., Osher, S., Zhao, H. and Kang, M. (1999). A PDE-based fast local level set method. *Journal of Computational Physics*, **155**(2), 410–438.

Rodi, W. (1993). *Turbulence models and their application in hydraulics*. CRC Press, New York, USA.

Satoru, K., Hiromasa, U., Fumimaru, O. and Tokuro, M. (1982). Turbulence structure and transport mechanism at the free surface in an open channel flow. *International Journal of Heat and Mass Transfer*, **25**(4), 513–521.

Schlichting, H. (1979). *Boundary-layer theory*. McGraw-Hill Book Company, New York, USA.

Sussman, M., Smereka, P. and Osher, S. (1994). A level set approach for computing solutions to incompressible two-phase flow. *Journal of Computational Physics*, **114**(1), 146–159.

Van der Vorst, H.A. (1992). Bi-CGSTAB: A fast and smoothly converging variant of Bi-CG for the solution of nonsymmetric linear systems. *SIAM Journal on scientific and Statistical Computing*, **13**(2), 631–644.

Wilcox, D. (1994). *Turbulence Modeling for CFD*. DCW Industries, Inc., La Canada, California. ISBN 9780963605108.

Wilcox, D.C. (1988). Reassessment of the scale-determining equation for advanced turbulence models. *AIAA journal*, **26**(11), 1299–1310.